RSC Advances

PAPER

View Article Online
View Journal | View Issue

Cite this: *RSC Adv.*, 2017, **7**, 44884

Unexpected stable stoichiometries and superconductivity of potassium-rich sulfides†‡

Ying Li, Xilian Jin,* Tian Cui,* Quan Zhuang, Die Zhang, Xing Meng, Kuo Bao, Bingbing Liu and Qiang Zhou

Received 6th July 2017
Accepted 22nd August 2017

DOI: 10.1039/c7ra07455g

rsc.li/rsc-advances

Alkali metal compounds exhibit novel characteristics under pressure, such as antimetallization in CLi_4, high superconductivity at 80 K in highly compressed Li_3S, and the existence of unexpected stable stoichiometries of sodium chlorides, *etc.*, which have greatly prompted us to explore K_xS compounds at pressure. We found several stable structures with a variety of stoichiometries and proposed a phase diagram on the K-rich side first. Chemical rules established at ambient pressure are frequently violated when high pressure is applied, Na_3Cl and $NaCl_3$ as unusual stoichiometries of sodium chloride have been reported in high-pressure conditions. However, KS, with its counterintuitive chemical formula, has been discovered theoretically even at ambient pressure, and possesses the same stability as K_2S. The mechanism of superconductivity in $Pm\bar{3}m$ K_3S is deeply investigated, comparing with the reported $Pm\bar{3}m$ Li_3S. The weak electron–phonon coupling mainly contributes to the weak superconductivity in K_3S, which is fully in contrast to the mechanism of interstitial charge localization which dominates the low T_c in the reported Li_3S.

Introduction

Recently, alkali metal compounds have revived the interest of the scientific community to explore their novel structures and characteristics upon compression. Different Na–Cl compounds such as Na_3Cl, Na_2Cl, Na_3Cl_2, $NaCl_3$, and $NaCl_7$ are thermodynamically stable at nonambient pressure conditions which contrasts the familiar rules of chemistry.[1,2] The compound of helium and sodium, Na_2He, reported recently has changed the hitherto bare field of helium chemistry, providing new twists to the chemistry of noble gases.[3] Antimetallization is predicted in the dense lithium-rich compound CLi_4 (ref. 4) which means that this phenomenon is expected in not only alkali metals Li[5–7] and Na[8] but also multiple compounds. Interestingly, superconductivity is predicted in alkali metal compounds such as a Li–S system, and T_c has risen to 80 K in highly compressed Li_3S.[9]

Alkali metal sulfides are characterized by their high ionic conductivity and large band gap. They appear to be promising candidates for technological applications in solid state batteries, fuel cells and solid state gas-detectors.[10,11] The properties of alkali metal sulfides of X_2S (X = Li, Na, K, or Rb) have been explored thoroughly, including phase sequence, elastic properties, electronic structure, optical properties, *etc.*[12–20] The conventional superconductivity in the phase diagram of the Li–S system has been explored by *ab initio* methods for crystal structure prediction and linear response calculations for electron–phonon coupling.[9] Most of these phases are metallic, but they exhibit no or low-T_c superconductivity, except for the $Fm\bar{3}m$ space group of Li_3S with a T_c of 80 K at 500 GPa. In contrast to the low-T_c of $Pm\bar{3}m$ Li_3S, it is concluded that interstitial charge localization due to avoiding core overlap can be a fundamental limiting factor for conventional superconductivity.

In this work, various stoichiometric structures of K_xS ($x = 1$–4) systems are widely investigated up to 100 GPa. We found six thermodynamically stable structures with the stoichiometries of KS, K_3S and K_4S under these conditions and proposed a phase diagram on the K-rich side first. KS, the totally counterintuitive chemical formula with extraordinary bonding and electronic properties, is predicted to be stable at atmospheric pressure in K_xS compounds. The mechanism of superconductivity in $Pm\bar{3}m$ K_3S is deeply investigated and compared with the reported $Pm\bar{3}m$ Li_3S. The low T_c is attributed to a weak interaction of electron–phonon coupling in the K_3S compound instead of interstitial charge localization like in the reported Li_3S compound.[9]

Computational methods

The structural prediction for the K_xS compounds at different pressures was performed by the ELocR code.[21] The high accuracy structural relaxations and electronic localization functions (ELF) were performed using density functional theory with the

College of Physics, State Key Laboratory of Superhard Materials, Jilin University, Changchun, 130012, People's Republic of China. E-mail: jinxilian@jlu.edu.cn; cuitian@jlu.edu.cn

† Dedicated to Prof. Guangtian Zou on the occasion of his 80th birthday.

‡ Electronic supplementary information (ESI) available. See DOI: 10.1039/c7ra07455g

Vienna ab initio simulation package (VASP).[22] The Perdew–Burke–Ernzerhof (PBE) generalized gradient approximation (GGA)[23] was selected for the exchange–correlation function. The partial augmented wave (PAW)[24] method was adopted with the PAW potentials where s^2p^4 and $3s^3p^4$s are treated as valence electrons. Brillouin zone sampling used a grid spacing of $2\pi \times 0.03$ Å^{-1} and the plane-wave cutoff energy was 600 eV.

The electronic projected density of states and the electronic band structure were calculated by the CASTEP[25] code with a cutoff energy of 720 eV, norm-conserving pseudopotentials, GGA-PBE exchange–correlation functional, and Brillouin zone sampling grid with a spacing of $2\pi \times 0.04$ Å^{-1}. The dynamic properties, three-dimensional Fermi surfaces and electron–phonon coupling calculations were studied in the QUANTUM-ESPRESSO package.[26] The Troullier–Martins-type norm-conserving pseudopotentials were used, and convergence tests provided a suitable value of 60 Ry for the kinetic energy cutoff. The q-point meshes in the first Brillouin zone of $8 \times 8 \times 8$ for $Pm\bar{3}m$ (Li_3S) and $4 \times 4 \times 4$ for $Pm\bar{3}m$ (K_3S) were used for phonon and electron–phonon calculations.

Results and discussion

We have systematically studied the chemical stabilities of various K_xS ($x = 1$–4) compounds by calculating the enthalpies of formation up to 100 GPa. The thermodynamical stability of different compounds with respect to elemental K and S solids at each pressure is calculated using the equation below:

$$\Delta H(K_xS) = [[H(K_xS) - xH(K) - H(S)]/(x + 1)]$$

where ΔH is the enthalpy of formation per atom and H is the calculated enthalpy per chemical unit for each compound. All possible structures with lower enthalpies are provided in the convex hull, as shown in Fig. 1 and S1.‡

According to the hull data, a compound lying on the convex hull is thermodynamically stable with respect to decomposition into other K–S compounds or elemental K and S solids, and thus it is experimentally synthesizable. However, those located above the convex hull indicated by dashed lines are either unstable or metastable. In order to obtain clear information for the structures at ambient conditions and 10 GPa, the independent convex hull is shown in Fig. S1.‡ Moreover, the phase diagram for the K_xS crystals is presented in Fig. 2.

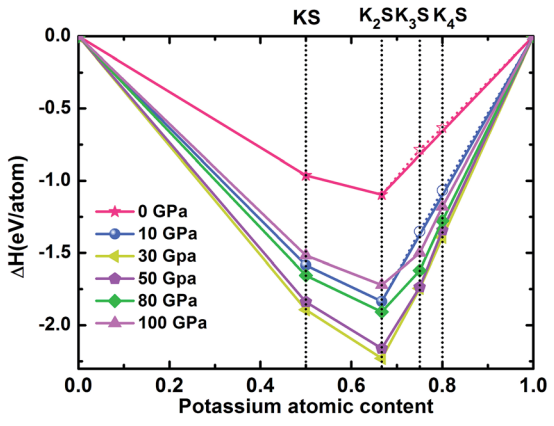

Fig. 1 Enthalpy difference curves of K_xS with respect to K and S at selected pressures. The K_xS structures on the convex hull (solid lines) are thermodynamically stable relative to decomposition into other K_xS compounds and elements, whereas those located above the convex hull (dashed lines) are unstable or metastable.

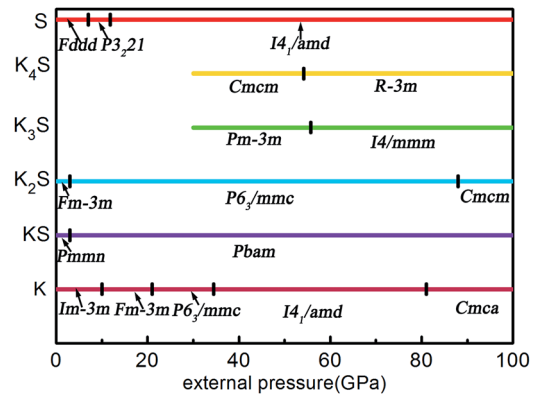

Fig. 2 The phase diagram of the K_xS system in the stable pressure range.

Under ambient conditions, the stable phase of KS crystallizes in the orthorhombic structure of *Pmmn* and remains stable until 3 GPa as shown in Fig. 3(a). There are three nonequivalent atoms, and the nearest distance between K and S is 3.16 Å. K atoms occupy the crystallographic 2b position with *mm*2 symmetry on the top and bottom sides, and the other nonequivalent K atoms occupy the crystallographic 2a position with *mm*2 symmetry in the middle of the crystal. S atoms occupy the crystallographic 4f position with *.m.* symmetry. Elevating the pressure above 3 GPa, another orthorhombic phase with *Pbam* symmetry emerges which is stable until 100 GPa, as depicted in Fig. 3(b). There are two nonequivalent atoms in the crystal lattice, and they consist of one KS unit. K atoms occupy the crystallographic 4h position with *..m* symmetry, and S atoms occupy the crystallographic 4g position with *..m* symmetry. The nearest distance between K and S is 2.558 Å. As for K_3S and K_4S, they are thermodynamically metastable under normal conditions until 30 GPa. With increasing pressure, $Pm\bar{3}m$, the face-centered cubic phase, is energetically preferred from 30 GPa

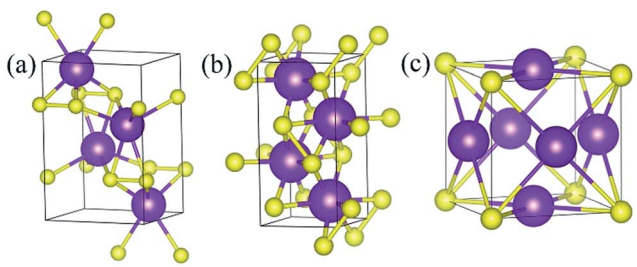

Fig. 3 Stable structures of K_xS: (a) *Pmmn* KS at ambient pressure, (b) *Pbam* KS at 100 GPa, and (c) $Pm\bar{3}m$ K_3S at 50 GPa. The purple and yellow atoms are K and S, respectively.

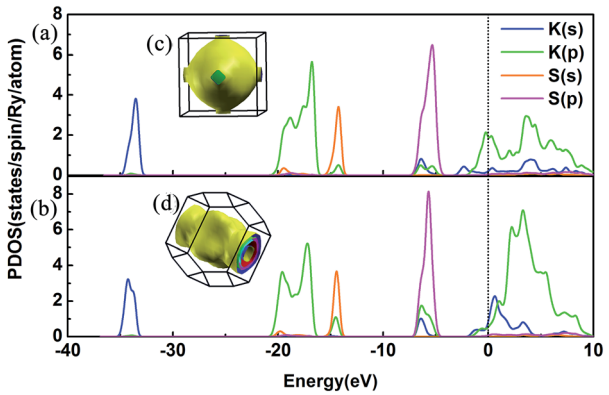

Fig. 4 PDOS and the three-dimensional Fermi surfaces of K_3S. (a) PDOS of $Pm\bar{3}m$ at 50 GPa, (b) PDOS of $I4/mmm$ at 100 GPa, (c) the three-dimensional Fermi surfaces of $Pm\bar{3}m$ at 50 GPa, and (d) the three-dimensional Fermi surfaces of $I4/mmm$ at 100 GPa. The black vertical dashed line indicates the Fermi energy.

to 55.7 GPa. The layer stacking sequence in every axis can be denoted by the repeated AB stacking. K atoms occupy the crystallographic 3c position with $4/mm.m$ symmetry sitting at the center of each cube face. S atoms occupy the crystallographic 1a position with $m\bar{3}m$ symmetry around the cube corners as shown in Fig. 3(c). Each K atom is surrounded by the four nearest S atoms and the distance is 2.779 Å. The calculated structural parameters and Wyckoff positions for each phase are summarized in Table S1.‡ The mechanical property is one of the basic criteria when considering the structure stability. According to the mechanical stability criteria, the crystal deformation energy is positive which means the determinants of the elastic constants matrix C_{ij} should be positive.[27] It is noteworthy that negative values are not prohibited for C_{ij}.[28] To evaluate the mechanical stability of *Pmmn*, *Pbam*, $Pm\bar{3}m$, $I4/mmm$, *Cmcm* and $R\bar{3}m$, the elastic constants were calculated and are listed in Table S2.‡ They all satisfy the Born–Huang criterion,[29] representing the stability of the mechanical property.

KS and K_2S are thermodynamically stable compounds throughout the entire pressure range we explored. At ambient pressure, K_2S is the familiar stoichiometry in the K_xS system. We have predicted its phase sequence successfully by the ELocR[21] code, and account for the experimental results effectively.[20] Pressure can efficiently modify the compositional landscape, leading to materials with unprecedented stoichiometries that would not be expected from conventional wisdom based on chemical rules at ambient pressure. For instance, at ambient conditions, sodium chloride (NaCl) is the archetypical ionic compound in chemistry textbooks. Under pressure, different Na–Cl compounds such as Na_3Cl, Na_2Cl, Na_3Cl_2, $NaCl_3$, and $NaCl_7$, which are clearly against our conventional wisdom, become thermodynamically stable.[1,2] Some other examples are seen in Li–B,[30,31] Ca–H,[32] and Si–C[33] systems at high pressure conditions. Interestingly, the unusual stoichiometry (1 : 1) KS compound is even stable thermodynamically and mechanically at ambient conditions. In order to judge its dynamical stability, the phonon band structure and partial phonon density of states (PHDOS) were calculated as shown in Fig. S2.‡ The absence of imaginary frequency modes in the entire Brillouin zone indicates the dynamic stability of *Pmmn* (KS). Hence, KS, the totally counterintuitive chemical formula, may exist in nature theoretically.

We have discussed the mechanical and thermodynamical stability of the proposed phases and confirmed that they are all stable at the relevant pressure range. To understand the electronic properties of the various K_xS compounds, the electronic band structures, partial density of states (PDOS) and three-dimensional Fermi surfaces were calculated as depicted in Fig. 4 and S3.‡ From the band structures we found that all the stable phases at the different pressures are metallic due to several bands crossing the Fermi level, except for *Pmmn* and *Pbam*. At ambient pressure, the band gap in *Pmmn* is 1.432 eV, which reveals its nonmetallic character. Elevating the pressure above 3 GPa, the *Pbam* structure appears with nonmetallic features until 100 GPa. For K_3S, from the partial density of states (PDOS) in Fig. 4(a) and (b), the metallic character of $Pm\bar{3}m$ and $I4/mmm$ is confirmed by the high level of total electronic density distribution at the Fermi level. The majority of the occupied states come from the K(p) state, whereas the contribution from

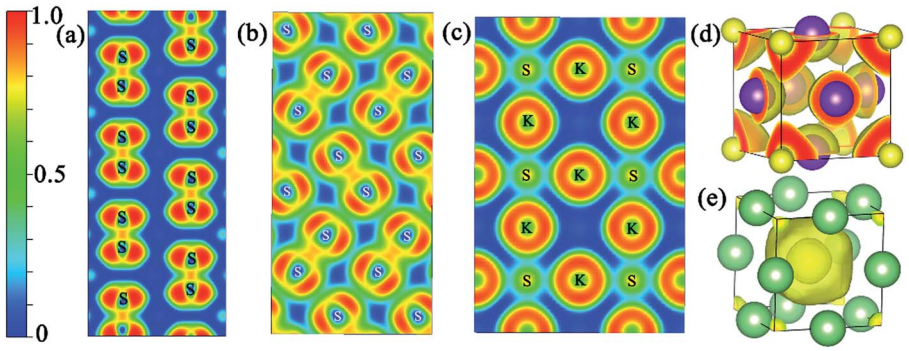

Fig. 5 The electron localization function of KS, K_3S and Li_3S. (a) *Pmmn* 2D ELF slice along the (011) plane at ambient pressure; (b) *Pbam* 2D ELF slice along the (001) plane at 100 GPa; (c) $Pm\bar{3}m$ K_3S 2D ELF slice along the (001) plane at 50 GPa; (d) $Pm\bar{3}m$ K_3S 3D ELF map with the ELF values of 0.65 at 50 GPa; (e) $Pm\bar{3}m$ Li_3S 3D ELF map with the ELF values of 0.65 at 500 GPa. $Pm\bar{m}$ Li_3S 3D ELF map with the ELF values of 0.65 at 500 GPa.

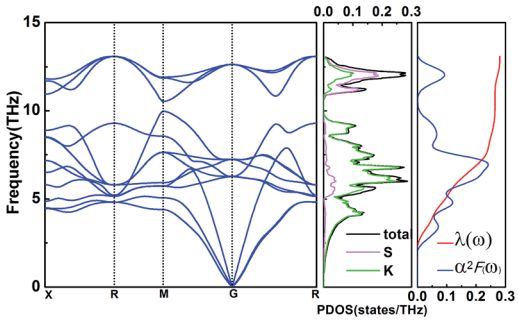

Fig. 6 Phonon dispersion curves, partial phonon density of states (PDOS), Eliashberg spectral function $\alpha^2F(\omega)$, and the EPC λ for $Pm\bar{3}m$ (K_3S) at 50 GPa.

K(s), S(s) and S(p) to the states around the Fermi level is quite small in K_3S. This complex electronic band structure near the Fermi energy brings the rich and multiple Fermi surface feature, as displayed in Fig. 4(c) and (d).

In addition, the electron localization function (ELF) was calculated to analyze the nature of the chemical bonding and the unusual distribution of the valence electron localization function in the proposed structures at the relevant pressure range. It is a ratio from 0 to 1, and the values equal 1.0 and 0.5, reflecting the extremely strong localization and homogeneous electron distribution, respectively.[34,35] Fig. S4‡ shows the isosurface value of 0.65 for the proposed structures. The valence electron localization around interstitial regions is found in *Pmmn* (KS), *Pbam* (KS), *I*4/*mmm* (K_3S), *Cmcm* (K_4S), and $R\bar{3}m$ (K_4S), and is not found in $Pm\bar{3}m$ (K_3S). Fig. 5(a) and (b) show the two dimensional electron location function (2D ELF) of *Pmmn* (KS) and *Pbam* (KS). The values around the positions of the S_2 units are close to 0.75, revealing the covalent bond character. From the 2D ELF of $Pm\bar{3}m$ (K_3S) displayed in Fig. 5(c), we can see that the conductivity comes from connected regions where the value of ELF is about 0.5 between the K and S atoms. The ELF of $Pm\bar{3}m$ (Li_3S) at 500 GPa is calculated to compare with K_3S as shown in Fig. 5(e). Obviously, charges accumulate in the open interstitial regions in Li_3S. However, this phenomenon is not observed in $Pm\bar{3}m$ K_3S as displayed in Fig. 5(d).

To explore the potential superconductivity of $Pm\bar{3}m$ K_3S, the electron–phonon coupling (EPC) strength λ and logarithmic average phonon frequency ω_{log} have been investigated at 50 GPa by QUANTUM-ESPRESSO.[26] The Eliashberg phonon spectral function $\alpha^2F(\omega)$ can be obtained as below. It is described as:

$$\alpha^2F(\omega) = \frac{1}{2\pi N(\varepsilon_F)} \sum_{qv} \frac{\gamma_{qv}}{\omega_{qv}} \delta(\omega - \omega_{qv}) \quad (1)$$

hereinto the line width:

$$\gamma_{qv} = \lambda_{qv} \pi N(\varepsilon_F) {\omega_{qv}}^2 \quad (2)$$

so, we can obtain $\alpha^2F(\omega)$:

$$\alpha^2F(\omega) = \frac{1}{2} \sum_{qv} \lambda_{qv} \omega_{qv} \delta(\omega - \omega_{qv}) \quad (3)$$

In this work, $\alpha^2F(\omega)$ is obtained by the integration of ω_{qv} in the whole Brillouin zone. The heavier K atom from the low-frequency vibrational modes below about 8 THz contributes more to the total λ as shown in Fig. 6. Phonon-mediated superconductors are accurately described by the Migdal–Eliashberg theory,[36,37] and T_c can be estimated by the Allen–Dynes formula:[38]

$$T_c = \frac{\omega_{log}}{1.2} \exp\left[\frac{-1.04(1+\lambda)}{\lambda - \mu^*(1+0.62\lambda)}\right] \quad (4)$$

which has been found to be highly accurate for many materials with $\lambda < 1.5$. We chose the better recommended values of the Coulomb pseudopotential μ^* (0.1–0.13),[39] and the superconducting transition temperature T_c was estimated to nearly 0 K at 50 GPa. A recent theoretical study reported that Li_3S exhibits low-T_c (0 K) in the $Pm\bar{3}m$ phase and high-T_c (80 K) in the $Fm\bar{3}m$ phase, and it attributed the difference to interstitial charge localization, *i.e.*, charge localizing in the interstitial region is a limiting factor to conventional superconductivity.[9] K_3S has the same stoichiometry, space group and T_c as Li_3S, however, the mechanism of superconductivity is totally different. We attribute the low T_c to weak electron–phonon coupling. As expected, in K_3S and Li_3S, T_c is dominated by λ. Then the variation of λ is analysed using the rigid-muffin-tin (RMT) theory of Gaspari and Gyorffy.[40] McMillan's strong coupling theory defines an electron–phonon coupling constant by

$$\lambda = \frac{N(\varepsilon_F)\langle I^2\rangle}{M\langle\omega^2\rangle} = \eta N(\varepsilon_F) \quad (5)$$

where $\eta = \frac{\langle I^2\rangle}{M\langle\omega^2\rangle}$. $N(\varepsilon_F)$ is the density of states (DOS) at the Fermi level, M is the atomic mass, $\langle\omega^2\rangle$ is a weighted average of

Table 1 The calculated electronic density of states at the Fermi level $N(\varepsilon_F)$ (states/spin/Ry/atom), the logarithmic average phonon frequency ω_{log} (K), the average phonon frequency $\langle\omega^2\rangle^{1/2}$ (THz), the average over the Fermi surface of the electron–phonon matrix element $\langle I^2\rangle$ (eV $Å^{-1}$),^{2} the electron–phonon coupling parameters λ, and the superconducting critical temperatures T_c (K) of K_3S and Li_3S at 50 GPa and 500 GPa, respectively

	Phase	P (GPa)	T_c	ω_{log}	λ	$N(\varepsilon_F)$	η	$\langle\omega^2\rangle^{1/2}$	$\langle I^2\rangle$
Present work	$Pm\bar{3}m$ (K_3S)	50	0.069	285.569	0.280	2.107	0.133	40.698	2.884
Present work	$Pm\bar{3}m$ (Li_3S)	500	0.044	814.923	0.250	0.668	0.375	141.074	25.120
Other calculations	$Pm\bar{3}m$ (Li_3S)[9]	500	0	702	0.25	0.67	0.37		

the square of the phonon frequency, and $\langle I^2 \rangle$ is an average over the Fermi surface of the electron–phonon matrix element. From Table 1, η plays an important role in λ which further influenced the low T_c in Li_3S and K_3S. With regard to η, it is believed that η is a factor about the lattice and its value is influenced by interstitial charge localization in Li_3S,[9] *i.e.* charge localizing in the interstitial region led to a smaller η. The value of η in K_3S is smaller than that in Li_3S, nevertheless, there is no charge localizing in the interstitial region as shown in Fig. 5(c). We attribute the small η to the electron–ion matrix element $\langle I^2 \rangle$. In conclusion, the low T_c in K_3S is mainly influenced by electron–phonon coupling which is fully in contrast to the mechanism of interstitial charge localization which dominates the low T_c in the reported Li_3S.[9]

Conclusions

In conclusion, a high-pressure phase diagram of K-rich K_xS systems was built from structure prediction simulations and first-principles calculations. KS, the totally counterintuitive chemical formula with extraordinary bonding and electronic properties, is predicted to be stable at atmospheric pressure. All of the S atoms of KS are in the form of S_2 units with covalent bond character from the analyses of the electronic localization function. Further electron–phonon coupling calculations revealed that the T_c of $Pm\bar{3}m$ (K_3S) is approximately near to 0 K at 50 GPa. The mechanism of superconductivity in $Pm\bar{3}m$ K_3S was deeply investigated and compared with the reported $Pm\bar{3}m$ Li_3S. We attribute the low T_c to weak electron–phonon coupling in the K_3S compound.

Conflicts of interest

There are no conflicts to declare.

Acknowledgements

This work was supported by the National Natural Science Foundation of China (No. 51632002, 51572108, 11634004, 11174102, 11774119), the Program for Changjiang Scholars and Innovative Research Team in University (No. IRT_15R23), the 111 Project (No. B12011), the National Fund for Fostering Talents of Basic Science (No. J1103202), and the Development Program of Science and Technology of Jilin Province, China (No. 20150312002ZG). Parts of the calculations were performed in the High Performance Computing Center (HPCC) of Jilin University.

References

1 W. Zhang, A. R. Oganov, A. F. Goncharov, *et al.*, *Science*, 2013, **342**, 1502–1505.
2 J. I. Insa, *Science*, 2013, **342**, 1459–1460.
3 X. Dong, A. R. Oganov, A. F. Goncharov, *et al.*, *Nat. Chem.*, 2017, **9**, 440–445.
4 X. Jin, X. J. Chen, T. Cui, H. K. Mao, H. Zhang, Q. Zhuang, K. Bao, D. Zhou, B. Liu, Q. Zhou and Z. He, *Proc. Natl. Acad. Sci. U. S. A.*, 2016, **113**, 2366–2369.
5 J. B. Neaton and N. W. Ashcroft, *Nature*, 1999, **400**, 141–144.
6 T. Matsuoka and K. Shimizu, *Nature*, 2009, **458**, 186–189.
7 Y. Yao, S. T. John and D. D. Klug, *Phys. Rev. Lett.*, 2009, **102**, 115503.
8 Y. Ma, M. Eremets, A. R. Oganov, *et al.*, *Nature*, 2009, **458**, 182–185.
9 C. Kokail, C. Heil and L. Boeri, *Phys. Rev. B*, 2016, **94**, 060502.
10 P. G. Bruce, S. A. Freunberger, L. J. Hardwick and J. Tarascon, *Nat. Mater.*, 2012, **11**, 19–29.
11 H. Momida, T. Yamashita and T. Oguchi, *J. Phys. Soc. Jpn.*, 2014, **83**, 124713.
12 H. Khachai, R. Khenata and A. Bouhemadou, *Solid State Commun.*, 2008, **147**, 178–182.
13 R. D. Eithiraj, G. Jaiganesh and G. Kalpana, *Phys. Status Solidi A*, 2007, **244**, 1337–1346.
14 J. C. Schön, Ž. Čančarević and M. Jansen, *J. Chem. Phys.*, 2004, **121**, 2289.
15 H. Khachai, R. Khenata and A. Bouhemadou, *J. Phys.*, 2009, **21**, 095404.
16 E. Zintl, A. Harder and B. Dauth, *Z. Elektrochem. Angew. Phys. Chem.*, 1934, **40**, 588–593.
17 A. Grzechnik, A. Vagas, K. Syassen, L. Loa, M. Hanfland and M. Jansen, *J. Solid State Chem.*, 2000, **154**, 603–611.
18 A. Vegas, A. Grzechnik, K. Syassen, L. Loa, M. Hanfland and M. Jansen, *Acta Crystallogr., Sect. B: Struct. Sci.*, 2001, **57**, 151–156.
19 D. Santamaria-Perez, A. Vegas, C. Muehle and M. Jansen, *Acta Crystallogr., Sect. B: Struct. Sci.*, 2011, **67**, 109–115.
20 Y. Li, X. Jin, T. Cui, Q. Zhuang, Q. Lv, G. Wu, X. Meng, K. Bao, B. Liu and Q. Zhou, *RSC Adv.*, 2017, **7**, 7424–7430.
21 The code for crystal structural prediction and analysis is based on the evolutional local random computational method, and is developed by our group. Some details have been provided in the ESI.‡
22 G. Kresse and J. Furthmüller, *Phys. Rev. B: Condens. Matter Mater. Phys.*, 1996, **54**, 11169–11186.
23 J. P. Perdew, K. Burke and M. Ernzerhof, *Phys. Rev. Lett.*, 1997, **77**, 3865–3868.
24 P. E. Blöchl, *Phys. Rev. B: Condens. Matter Mater. Phys.*, 1994, **50**, 17953–17979.
25 S. J. Clark, M. D. Segall and C. J. Pickard, *Z. Kristallogr. - Cryst. Mater.*, 2005, **220**, 567–570.
26 P. Giannozzi, S. Baroni, N. Bonini, M. Calandra, R. Car, C. Cavazzoni, D. Ceresoli, G. L. Chiarotti, M. Cococcioni, I. Dabo, A. Dal Corso, S. de Gironcoli, S. Fabris, G. Fratesi, R. Gebauer, U. Gerstmann, C. Gougoussis, A. Kokalj, M. Lazzeri, L. Martin-Samos, N. Marzari, F. Mauri, R. Mazzarello, S. Paolini, A. Pasquarello, L. Paulatto, C. Sbraccia, S. Scandolo, G. Sclauzero, A. P. Seitsonen, A. Smogunov, P. Umari and R. M. Wentzcovitch, *J. Phys.: Condens. Matter*, 2009, **21**, 395502.
27 J. F. Nye, *Physical properties of crystals: their representation by tensors and matrices*, Oxford Univ. Press, Oxford, 1985, pp. 142–143.

28 J. P. Perdew and K. Burke, *Phys. Rev. Lett.*, 1997, **77**, 3865–3868.
29 Z. Wu, E. Zhao and H. Xiang, *Phys. Rev. B: Condens. Matter Mater. Phys.*, 2007, **76**, 054115.
30 F. Peng, M. Miao, H. Wang, Q. Li and Y. Ma, *J. Am. Chem. Soc.*, 2012, **134**, 18599–18605.
31 A. Hermann, A. McSorley, N. W. Ashcroft and R. Hoffmann, *J. Am. Chem. Soc.*, 2012, **134**, 18606–18618.
32 H. Wang, S. T. John, K. Tanaka, T. Iitaka and Y. Ma, *Proc. Natl. Acad. Sci. U. S. A.*, 2012, **109**, 6463–6466.
33 G. Gao, N. Ashcroft and R. Hoffmann, *J. Am. Chem. Soc.*, 2013, **135**, 11651–11656.
34 A. D. Becke and K. E. Edgecombe, *J. Chem. Phys.*, 1990, **92**, 5397–5403.
35 J. K. Burdett and T. A. McCormick, *J. Phys. Chem. A*, 1998, **102**, 6366–6372.
36 A. B. Migdal, *J. Exp. Theor. Phys.*, 1958, **34**, 996.
37 G. M. Eliashberg, *J. Exp. Theor.Phys.*, 1960, **11**, 696.
38 P. B. Allen and R. C. Dynes, *Phys. Rev. B: Solid State*, 1975, **12**, 905–922.
39 N. W. Ashcroft, *Phys. Rev. Lett.*, 2004, **92**, 187002.
40 G. D. Gaspari and B. L. Gyorffy, *Phys. Rev. Lett.*, 1972, **28**, 801–805.